

---

## A novel dual-fusion algorithm of single image dehazing based on anisotropic diffusion and Gaussian filter

---

Kaihan Xiao, Qingshan Tang\*, Si Liu and Sijie Li

School of Physics and Electronic Science,  
Changsha University of Science and Technology,  
Changsha, China

Email: 695422512@qq.com

Email: cstqs001@126.com

Email: liu.si@hotmail.com

Email: lisijie\_st@163.com

\*Corresponding author

Jiayi Huang

School of Computer Science and Information Engineering,  
Hubei University,  
Wuhan, China

Email: 2496700622@qq.com

Tao Huang

State-Owned Wuhan Changhong Machine Factory,  
Shidong Street, Wuchang District, Wuhan, China

Email: enghuangtao@126.com

**Abstract:** Dark channel prior (DCP) is a widely used method in single image dehazing technology. Here, we propose a novel dual-fusion algorithm of single image dehazing based on anisotropic diffusion and Gaussian filter to suppress the halo effect or colour distortion in traditional DCP algorithms. Anisotropic diffusion is used to edge-preserving smooth images and a Gaussian filter is to smooth the local white objects. A dual-fusion strategy is conducted to optimise the atmospheric veil. Besides, the fast explicit diffusion (FED) scheme is used to accelerate the numerical solution of the anisotropic diffusion to reduce time consumption. The subjective and objective evaluation of the experiment shows that the proposed algorithm can effectively suppress the halo effect and colour distortion, and has good dehazing performance on evaluation metrics. The proposed algorithm also reduces the time consumption by 54.2% than DCP with guided filter. This study provides an effective solution for single image dehazing.

**Keywords:** image dehazing; dark channel prior; DCP; anisotropic diffusion; fast explicit diffusion; FED; image fusion.

**Reference** to this paper should be made as follows: Xiao, K., Tang, Q., Liu, S., Li, S., Huang, J. and Huang, T. (2023) 'A novel dual-fusion algorithm of single image dehazing based on anisotropic diffusion and Gaussian filter', *Int. J. Computational Science and Engineering*, Vol. 26, No. 1, pp.54–64.

**Biographical notes:** Kaihan Xiao is a postgraduate student in the School of Physics and Electronic Science, Changsha University of Science and Technology, Changsha, China. His research interests include image processing and computer vision.

Qingshan Tang received his PhD in Signal and Information Processing from The Institute of Acoustics of the Chinese Academy of Sciences, Beijing, China in 2009. He is a Lecturer at the Changsha University of Science and Technology, China. His current research interests include array signal processing and image processing.

Si Liu received her PhD in Microelectronics and Solid-State Electronics from the Wuhan University, Wuhan, China, in 2012. From 2017 to 2018, she worked as a visiting scholar with The University of Texas at Dallas (UTD). She is a Lecturer at the Changsha University of Science and Technology, China. Her current research interests include interspace magnetic field detecting and image processing.

Sijie Li is a postgraduate student in the School of Physics and Electronic Science, Changsha University of Science and Technology, Changsha, China. His research interests include image processing.

Jiayi Huang is an undergraduate in the School of Computer Science and Information Engineering, Hubei University, Wuhan, China. His research interests include image processing and computer software.

Tao Huang received his Master of Aerospace Engineering from Northwestern Polytechnical University, and he is an employee in State-Owned Wuhan Changhong Machine Factory, Wuhan, China. His research interests include photoelectric image processing and computer vision.

## 1 Introduction

The problem of air pollution is increasingly serious worldwide, with the rapid development of industry (Chang et al., 2021). Hazy atmospheric conditions are therefore occurring increasingly frequently. In the hazy weather, light reflected off objects and received by a visual imaging system (Kholerdi et al., 2016; Zhao et al., 2021) is absorbed and scattered by the scattered particles in the air, and is also affected by the scattering of atmospheric light, resulting in the degradation of the image. This degradation affects the performance of visual tasks (Wei et al., 2016; Zhu et al., 2020; Sun et al., 2021). Therefore, image dehazing is a necessary pre-processing step when performing visual tasks on hazy days (Wu et al., 2019; Jiang et al., 2021; Das and Chand, 2021).

Image dehazing methods can be classified into two categories.

- 1 Those based on image enhancement, as histogram equalisation (Xu et al., 2009; Xu and Zhang, 2020), Retinex (Land and McCann, 1971), and homomorphic filter (Seow and Asari, 2006).
- 2 Those based on image restoration. The first class ignores the causes of hazy image generation, while the second class adopts an atmospheric scattering model (ASM) to describe the hazy image generation and the image degradation model used in dehazing (McCartney, 1976; Narasimhan and Nayar, 2002).

The second class of methods based on image restoration has attracted the most attention in the research community. Dehazing methods based on prior information are typical image restoration approaches.

Dark channel prior (DCP) proposed by He et al. (2010), is the most influential approach to prior information. DCP assumes that at least one colour channel has very low pixel value intensity in the clear image's non-sky, and no white object patches. The initial transmission can therefore be estimated using a minimum filter. However, the minimum filter may destroy the edges of the image, and cause the halo effect. The soft matting (SM) method was developed to reduce the halo effect. However, SM cannot be applied to high-resolution images, due to the complexity. He et al. (2013) proposed a guided filter (GF) to replace SM. GF improves the speed of DCP, but its performance on the

suppression of halo is worse than that of SM. Several other algorithms have also been developed as improvements on the DCP (Wei et al., 2020; Yang et al., 2021; Ehsan et al., 2021). Tarel and Hautière (2009) applied a series of median filters replacing the minimum filter, to reduce the halo effect, but this algorithm introduces many new false edges and causes colour distortion. Tripathi and Mukhopadhyay (2012) refined the atmospheric veil using anisotropic diffusion. This algorithm performs well in suppressing the halo effect, but leads to colour distortion in local white objects. Nandal and Kumar (2019) used fractional-order anisotropic diffusion instead of anisotropic diffusion to optimise the atmospheric veil. This algorithm solves the anisotropic diffusion equation in the spatial domain and reduces the time consumption, but still does not avoid colour distortion. In addition to DCP, many novel dehazing methods based on prior information have been proposed in recent years, such as colour attenuation prior (Zhu et al., 2015), haze-lines prior (Berman et al., 2020), colour ellipsoid prior (Bui and Kim., 2018) and gamma correction prior (Ju et al., 2020). The rough transmission was estimated based on these hypotheses. These algorithms require post-processing to refine the initial transmission.

To address the problem of the halo effect and colour distortion, we propose a dual-fusion dehazing algorithm based on anisotropic diffusion and Gaussian filter in this paper. The core idea of our work is to develop an efficient and practical image dual-fusion algorithm. The proposed algorithm does not need a GF, image regularisation method, or other complex methods, just uses twice image fusion can obtain the optimised atmospheric veil. Anisotropic diffusion is the most complex part of the proposed algorithm. We apply a novel fast explicit diffusion (FED) scheme to speed up the numerical solution. FED scheme can greatly reduce computational expense and improve efficiency. More specifically, in order to improve the accuracy of atmospheric light estimation, we use a search method based on the quadtree search. To reduce the halo effect and colour distortion, an anisotropic diffusion and Gaussian filter are used to the image of the minimal component respectively. The purpose of the anisotropic diffusion is to obtain an atmospheric veil with edge-preserving and smooth details, and the Gaussian filter is to smooth the local white object. The optimised atmospheric veil is obtained using a dual-fusion strategy. The first image fusion is used to correct the

colour distortion and the second is used to suppress the halo effect on image depth edges. Finally, a simple correction method is used to correct the minimum value of the optimised atmospheric veil.

The main contributions of the proposed algorithm can be summarised as follows. Firstly, to solve the colour distortion and halo effect, a novel and efficient dual-fusion strategy based on the Gaussian filter and anisotropic diffusion is used to optimise the atmospheric veil. Secondly, we use the FED scheme to speed up the numerical solution of anisotropic diffusion and improve the efficiency of the proposed algorithm.

The rest of the paper is structured as follows. The background to dehazing techniques and anisotropic diffusion is presented in Section 2. Section 3 describes our dual-fusion algorithm. The experimental results and analysis are given in Section 4. In the last section, Section 5, we conclude the work.

## 2 Background

In Section 2, we introduce the concepts of image dehazing technology and anisotropic diffusion, which are important in the framework of the proposed algorithm.

### 2.1 Atmospheric scattering model

In the domain of image processing, ASM is widely applied in image dehazing research based on image restoration (Narasimhan and Nayar, 2002). The basic model can be described as follows:

$$I(x, y) = J(x, y)t(x, y) + A[1 - t(x, y)] \quad (1)$$

$$t(x, y) = e^{-\beta d(x, y)} \quad (2)$$

where  $I$  denotes the hazy image,  $J$  is the original clear image,  $A$  is the value of atmospheric light and  $t$  is the transmission. Transmission is related to the scattering coefficient  $\beta$  and the image depth  $d$ .

In equation (1), assuming  $V(x, y) = A[1 - t(x, y)]$ , so the second term  $V$  is called the atmospheric veil. The atmospheric veil  $V$  is smooth as a whole, but the edge is clear at the change of image depth. The atmospheric veil  $V$  satisfies the following constraints (Tarel and Hautière, 2009):

$$0 \leq V(x, y) \leq W(x, y) \quad (3)$$

where  $W(x, y)$  is the minimal component in all colour channels of the hazy image,  $W(x, y) = \min I^c(x, y)$ . From the atmospheric veil, the transmission can be deduced as follows:

$$t(x, y) = 1 - \omega \frac{V(x, y)}{A} \quad (4)$$

The constant parameter  $\omega$  is used to control the degree of dehazing, and we used a value of  $\omega$  of 0.95 for all

experiments in this paper. We can obtain a haze-free image using:

$$f(x, y) = \frac{I(x, y) - A}{\max[t(x, y), t_0]} \quad (5)$$

where the lower bound of  $t$  is  $t_0$ , avoiding zero in the denominator. We chose 0.01 as a typical value of  $t_0$ .

### 2.2 Dark channel prior

He et al. (2010) analysed numerous clear and haze-free outdoor images and proposed the concept of DCP. DCP assumes that at least one colour channel has very low pixel value intensity in the clear image's non-sky and no white object patches. The mathematical expression is as follows:

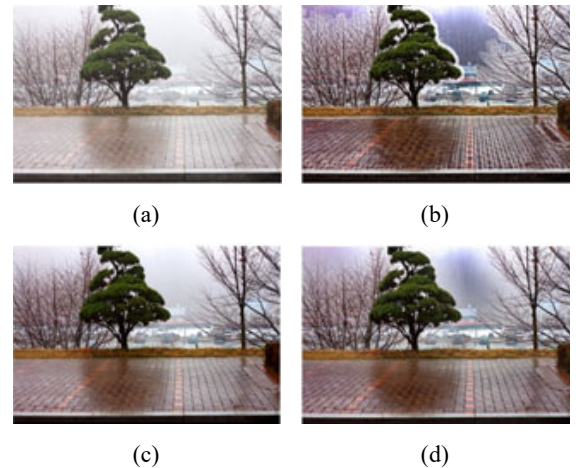
$$J^{dark}(x, y) = \min_{y \in \Omega(x, y)} \left( \min_{c \in \Omega\{R, G, B\}} (J^c(x, y)) \right) \rightarrow 0 \quad (6)$$

where  $J^{dark}(x, y)$  is called the dark channel, and  $\Omega(x, y)$  is a local patch centred at pixel  $(x, y)$ . Combining with equations (1) and (6), we can get:

$$\tilde{t}(x, y) = 1 - \min_{y \in \Omega(x)} \left( \min_{c \in \Omega\{R, G, B\}} \left( \frac{I^c(x, y)}{A^c} \right) \right) \quad (7)$$

where  $\tilde{t}(x, y)$  denotes the initial transmission. Compared with equation (4), we can see that the minimum filter is applied to erode  $W$  to estimate the atmospheric veil  $V$ . In order to suppress the halo effect caused by the minimum filter, He et al. (2010) and He et al. (2013) proposed the SM and GF methods to refine the initial transmission. The dehazing results of DCP are shown in Figure 1.

**Figure 1** Dehazing results of DCP, (a) hazy image, (b) initial transmission, (c) refined by SM, (d) refined by GF (see online version for colours)



### 2.3 Anisotropic diffusion

#### 2.3.1 Perona-Malik (P-M) filter

In the domain of image processing, anisotropic diffusion is commonly applied to reduce image noise or texture details without removing significant image edges. In general, the

term anisotropic diffusion refers to the P-M filter (Perona and Malik, 1990). The P-M filter can be represented as:

$$\frac{\partial I(x, y, T)}{\partial T} = \text{div}(g(|\nabla I|) \cdot \nabla I) \quad (8)$$

where  $\text{div}$  is a divergence operator and  $T$  is the diffusion time, and  $\nabla$  is the gradient operator. The function  $g$  is known as the conductivity function. In the P-M equation, the conductivity function is a monotonically decreasing function of the image gradient. In this paper, the form of the conductivity function is as follows:

$$g(|\nabla I|) = \frac{1}{\left(\frac{|\nabla I|}{\lambda}\right)^2 + 1} \quad (9)$$

where  $\lambda$  is the factor that controls the level of diffusion. The range of the conductivity function is  $[0, 1]$ .

### 2.3.2 Fast explicit diffusion

The solution of the P-M equation is related to the conductivity function  $g$ . When  $g$  is equal to a constant, the P-M equation has an analytic solution, which is a Gaussian distribution function. In this case, the P-M filter is equivalent to a Gaussian filter. In other cases, the P-M equation is a partial differential equation that usually has only a numerical solution. Therefore, the choice of a numerical scheme will determine the time consumption of the algorithm. The general explicit scheme is easy to implement, but is limited by the maximum stable time step size. The semi-implicit scheme needs to solve large-scale linear equations, but it is less limited by the time step size.

We used the FED scheme to solve the P-M equation (Weickert et al., 2016). FED is an explicit scheme with varying time steps, which combines the advantages of an explicit scheme and a semi-implicit scheme, and avoids their disadvantages. The FED scheme divides the given diffusion time  $T$  into a specified number  $M$  of FED cycles, and each FED cycle has  $n$  varying time steps  $\tau_i$  ( $i = 0, \dots, n - 1$ ) obtained from the factorisation of a box filter. Half of the time steps violate the maximum stable step size condition, but the numerical scheme still converges. The two-dimensional FED scheme is:

$$\mathbf{I}^{k+1, i+1} = \left( E + \tau_i \sum_{l=1}^2 A_l(\mathbf{I}^k) \right) \mathbf{I}^{k+1, i} \quad (10)$$

where  $E$  denotes the identity matrix, the column vector  $\mathbf{I}$  is reshaped from the image matrix  $I$  and  $A_l(\mathbf{I}^k)$  is the matrix embedding the conductivity function and central difference scheme. With  $A(\mathbf{I}^k) = (a_{ij}(\mathbf{I}^k))$  and the definition is as follows (Weickert et al., 1998):

$$a_{ij}(\mathbf{I}^k) := \begin{cases} \frac{g_i^k + g_j^k}{2} & j \in \mathbb{N}(i) \\ -\sum_{n \in \mathbb{N}(i)} \frac{g_i^k + g_n^k}{2} & j = i \\ 0 & \text{else} \end{cases} \quad (11)$$

where  $g_i = g(\mathbf{I})$ ,  $\mathbb{N}(i)$  is the neighbourhood of the pixel in a single direction. The vary time step  $\tau_i$  in a FED cycle is:

$$\tau_i = \frac{3T}{2M(n^2 + n) \cos \left\lceil \frac{\pi(2i+1)}{4n+2} \right\rceil} \quad (12)$$

The number of varying time step  $n$  in a FED cycle is:

$$n = \left\lceil -\frac{1}{2} + \frac{1}{2} \cdot \sqrt{1 + \frac{12 \cdot T}{M \cdot \tau_{\max}}} \right\rceil \quad (13)$$

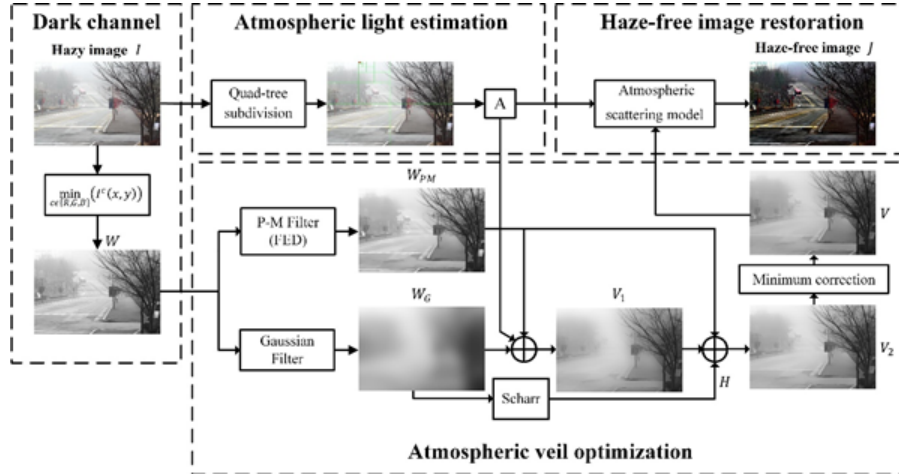
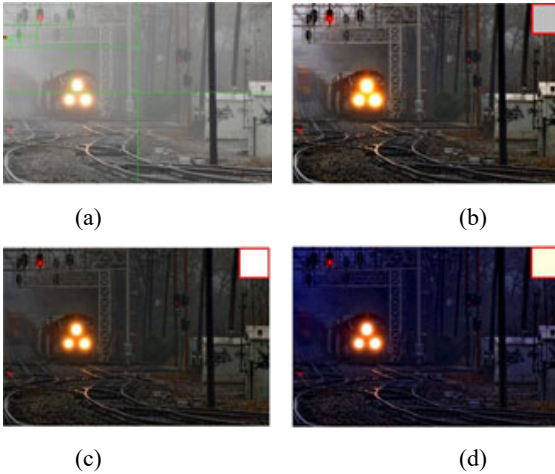
where the ceiling function  $\lceil x \rceil$  represents the minimum integer greater than  $x$ ,  $\tau_{\max}$  is the maximum stable time step size.

## 3 Proposed algorithm

In Section 3, the proposed novel dual-fusion algorithm of image dehazing algorithm based on anisotropic diffusion and Gaussian filter is described in detail. Firstly, we use a search method based on the quadtree search to find the reasonable pixel values for the atmospheric light. Then anisotropic diffusion and Gaussian filter are used to image of the colour channel minimal component respectively. A dual-fusion strategy is then used to optimise the atmospheric veil. The first image fusion is used to correct the colour distortion and the second is to suppress the halo effect in image depth edges. Finally, a simple correction method is used to correct the minimum value of the optimised atmospheric veil. Specifically, the proposed algorithm mainly includes the following two components: atmospheric light estimation and atmospheric veil optimisation. The flow chart of the proposed dehazing algorithm is shown in Figure 2.

### 3.1 Atmospheric light estimation

The DCP method selects the brightest 0.1% of pixels in the  $J^{\text{dark}}$  ( $x, y$ ), and finds the corresponding positions in the original hazy image. The pixel with the maximum pixel value in these positions is regarded as atmospheric light. The size of the minimum filter radius is an important parameter of DCP. When the filter radius is small, the local large white objects cannot be excluded from the dark channel, which may cause overestimation of the atmospheric light. When the filter radius is large, the dark channel is almost completely dark. In this case, the algorithm cannot find a reasonable pixel, which leads to an incorrect estimation of the atmospheric light.

**Figure 2** Flowchart of the proposed dehazing algorithm**Figure 3** Atmospheric light estimated using different methods, and dehazing results, (a) proposed method, (b) dehazing using the proposed method, (c) dehazing using He's method, (d) dehazing using Meng's method (see online version for colours)

Using observation and analysis, it was found that the variance between pixels is low in the sky and in thick fog regions. Therefore, we use a search method based on the quadtree search to estimate the atmospheric light (Kim et al., 2013). Firstly, we separate the hazy image into four rectangular regions of the same size, and then define a score function that is equal to the average of the pixel values minus the standard deviation in each given region. We select the highest score of the four regions and separate this region into four smaller regions. The above process is repeated until the selected region is smaller than a pre-set size threshold. In the last selected region, we find the pixel which is closest to pure white. This process is equivalent to finding the pixel which minimises the distance  $\|(I_R, I_G, I_B) - (255, 255, 255)\|$ . The estimated atmospheric light is the selected pixel value. Figure 3 shows the atmospheric light of the proposed algorithm and other algorithms, as well as the results of atmospheric light used to haze removal. He's method mistakenly regards the train lamp as the atmospheric light, making the restored image darker than the real image. Meng's method estimates atmospheric light

independently in each colour channel, instead of looking for pixels in the image to represent atmospheric light, which produces serious colour distortion in the restored image.

### 3.2 Atmospheric veil optimisation

The atmospheric veil  $V$  is smooth as a whole, but the edge is clear when the image depth changes. This effect is dependent upon the depth of the image, regardless of the colour of the object. Therefore, using the minimal component in all colour channels  $W$  to estimate the atmospheric veil should reduce the interference caused by local white objects. He's method uses the minimum filter to erode local white objects, but the minimum filter will destroy the image edge, resulting in the production of the halo effect.

Considering the characteristics of the atmospheric veil, the P-M filter is a feasible method (Tripathi and Mukhopadhyay, 2012; Nandal and Kumar, 2019). However, obvious white objects usually have clear edges, and a P-M filter with a low factor  $\lambda$  cannot smooth these local white objects, which may lead to colour distortion after dehazing. The images produced by these algorithms therefore usually need post-processing, e.g., histogram stretching and tone mapping.

#### 3.2.1 Dual-fusion optimisation strategy

We apply the dual-fusion strategy to reduce colour distortion and halo effect. First, a P-M filter with a low factor  $\lambda_1$  is used to smooth  $W(x, y)$ :

$$W(x, y, 0) = W(x, y,)$$
 (14)

$$\frac{\partial W(x, y, T)}{\partial T} = \text{div}(g(|\nabla W|) \cdot \nabla W)$$
 (15)

When the diffusion time  $T = T_1$ , the solution of equation (15) is  $W_{PM}$ .  $W_{PM}$  is shown in the in Figure 4(a). It has clear edge information, but contains less texture details. Because the Gaussian filter can be regarded as an unrestricted diffusion process, it can smooth local white

objects. The larger the standard deviation  $\sigma$ , the longer the diffusion time  $T$ , satisfying the equation  $T = 0.5 \sigma^2$ . When the image resolution is higher, the standard deviation of the corresponding Gaussian filter is larger. Therefore, we use a Gaussian filter with an adaptive standard deviation to smooth  $W(x, y)$  and get  $W_G$ . The adaptive standard deviation is related to the image resolution:

$$\sigma = \sqrt{2\sqrt{h \times w}} \quad (16)$$

where the  $h$  and  $w$  are the height and width of the image, respectively. This Gaussian filter corresponds to a homogeneous diffusion with diffusion time  $T = \sqrt{h \times w}$ . As we can observe in Figure 4(b),  $W_G$  can be regarded as a rough depth image without edge information.

To correct the colour distortion of local white objects, we performed the first image fusion between  $W_{PM}$  and  $W_G$ . The fusion image is the initial atmospheric  $V_1$ .  $V_1$  should contain some edge information, but the local white objects need to be corrected. The local white objects have similar pixel values to atmospheric light. When a pixel value in the  $W_{PM}$  is larger and closer to the atmospheric light, it means that the pixel is atmospheric light or local white objects. In the first case, the pixel is atmospheric light, and the same the position of  $W_G$  is also atmospheric light. In the second case, the pixel is located in the local white object, and the pixel in the same position of  $W_G$  is corrected by the Gaussian filter. Therefore, the component of  $W_G$  needs to be increased. The fusion coefficient of the first fusion is  $c_1$ :

$$c_1 = \min\left(1, \frac{W_{PM}}{\min A^c}\right) \quad (17)$$

where  $\min A^c$  denotes the minimum value of atmospheric light in all colour channels. When  $W_{PM}$  is close to  $\min A^c$ , the  $c_1$  is close to 1. The initial atmospheric veil  $V_1$  for the first image fusion is as follows:

$$V_1 = c_1 \times W_G + (1 - c_1) W_{PM} \quad (18)$$

The Gaussian filter destroys the depth information of the image. If  $W_G$  is used as the atmospheric veil to remove haze, it will produce serious halo effect. As we can see in Figure 4(b), the initial atmospheric veil  $V_1$  contains  $W_G$  component in the image depth edge. When  $V_1$  is used to remove haze, it will also appear halo effect. Through observation, it is found that the halo effect caused by the Gaussian filter and minimum filter is different. The blocking effect caused by the minimum filter will lead to the same intensity of halo in the same block. Figure 1(b) shows this halo effect. The halo caused by the Gaussian filter decreases gradually along the depth gradient and the change rates are similar. Therefore, we can use an image gradient operator to extract halo information  $H$  from  $W_G$ . The Scharr operator has stronger anti-interference and higher accuracy than the Sobel operator. The expression is as follows:

$$S_x = \begin{bmatrix} -3 & 0 & 3 \\ -10 & 0 & 10 \\ -3 & 0 & 3 \end{bmatrix} S_y = \begin{bmatrix} 3 & 10 & 3 \\ 0 & 0 & 0 \\ -3 & 10 & -3 \end{bmatrix} \quad (19)$$

where  $S_x$  and  $S_y$  are the gradient operators in the horizontal and vertical directions, respectively. The halo information  $H$  is Scharr operator's gradient magnitude:

$$H = \sqrt{(W_G \otimes S_x)^2 + (W_G \otimes S_y)^2} \quad (20)$$

where  $\otimes$  denotes the convolution operator. The second fusion coefficient  $c_2$  is obtained by normalising the halo information  $H$ :

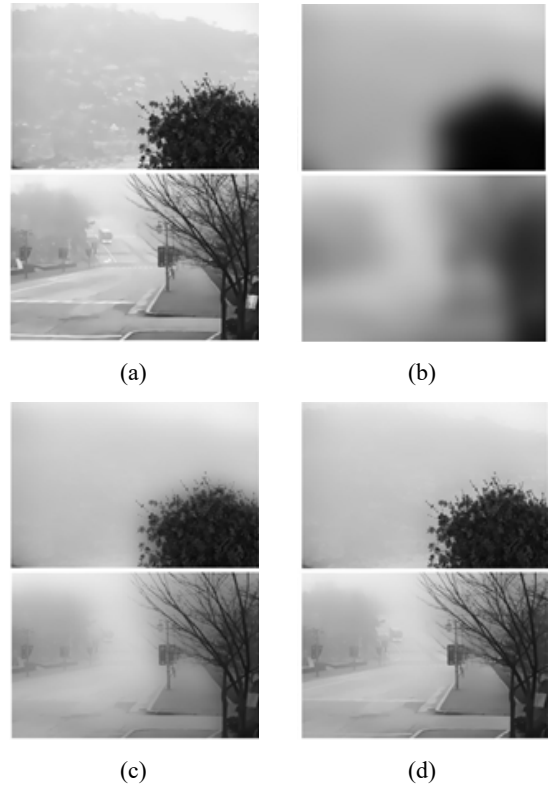
$$c_2 = H / \max(H) \quad (21)$$

When the pixels in the initial atmospheric veil  $V_1$  belong to halo, it has a high gradient magnitude. Therefore, it is necessary to increase the component of  $W_{PM}$  to restore the initial depth.  $V_1$  and  $W_{PM}$  are fused to get the atmospheric veil  $V_2$ :

$$V_2 = c_2 \times W_{PM} + (1 - c_2) \times V_1 \quad (22)$$

The second fusion image  $V_2$  is shown in Figure 4(d), we can see that the optimised atmospheric light has clear image depth edge and the local white objects are corrected.

**Figure 4** Optimisation of the atmospheric veil, (a)  $W_{PM}$ , (b)  $W_G$ , (c)  $V_1$ , (d)  $V_2$



### 3.2.2 Minimum value correction

The P-M filter and the Gaussian filter essentially involve pixel value diffusion. The sum of the pixel values in the

image does not change with the diffusion process, but the minimum and maximum values may change with the diffusion process. Therefore, the minimum value of the obtained atmospheric veil is larger than the minimal component in all colour channels  $W(x, y)$ , which may result in the low contrast in the restored image. We use a simple method to correct the minimum value of  $V_2$  to make it equal to the minimum value of  $W$ . The final optimised atmospheric veil  $V$  is:

$$V = V_2 - (\min V_2 - \min W) \quad (23)$$

Figure 4 shows the optimisation and results of the atmospheric veil.

Finally, we can apply the final optimised atmospheric veil  $V$  and the atmospheric light  $A$  in equations (4) and (5) to restore the haze-free image.

## 4 Experimental results and analysis

In order to verify the effectiveness of the proposed dehazing algorithm, we use a combination of subjective and objective evaluation method. We choose several natural images and synthetic images to test the algorithm, and compared the results with those of FVR (Tarel and Hautière, 2009), DCP-SM (He et al., 2010), DCP-GF (He et al., 2013), BCCR (Meng et al., 2013), CAP (Zhu et al., 2015), NLD (Berman et al., 2020), AARNCB (Dhara et al., 2020) and DTMS (Ehsan et al., 2021). In the above algorithm, the radius  $R$  of the minimum filter and morphological closing operation is fixed at to 15. The parameters of the proposed algorithm are initialised as follows:  $\lambda = 10$ ,  $T_1 = 50$ ,  $M = 2$ ,  $\tau_{\max} = 0.25$ . All the compared algorithms run in MATLAB R2018a on a personal computer with an Inter(R) Core (TM) i7-6700HQ CPU @ 2.60GHz, under a Windows10 64-bit operating system.

### 4.1 Subjective evaluation

For the dehazing algorithm, the subjective evaluation involved people's perceptions of the hazy images and restored clear images. The subjective evaluation criteria are related to the halo, colour distortion and contrast in the image. We adopt several widely used natural images in which the halo effect and colour distortion are easily induced. Figure 5 shows the dehazing results.

In Figure 5, the images are named lake, house, and canyon in turn. On the whole, DCP-SM and CAP have poor dehazing performance in the test image, and other algorithms have achieved a different level of dehazing performance. For the thick fog in the lake image, the restored images of DCP-GF, CAP and DTMS produced halo effect significantly. FVR, BCCR, NLD, and AARNCB produced residual haze at the edges of the image depth. The proposed algorithm and DCP-SM can restore the city scene in thick fog without halo effect. For the house image, the haze-free image restored by FVR has serious colour distortion. DCP-GF and CAP produced halo effect in the leaf edge, and the dehazing performance is poor. In the test

of canyon image, FVR produces many edge artefacts. NLD produced abnormal results for the sky, and does not restore the clouds. The DTMS is low brightness in the canyon region. In general, haze removal algorithms in which transmission was refined by GF, such as DCP-GF, CAP, and DTMS, are very prone to produce halo. FVR, BCCR, NLD, and AARNCB produce incomplete dehazing, possible because the regularisation or filter process could not preserve the image edges well. DCP-SM and the proposed dehazing algorithm can remove the haze and effectively suppress the halo effect.

Figure 6 shows an example of local white object correction. In Figures 6(h), 6(i), 6(j) and 6(k) respectively. When the filter radius  $R$  is small, the halo effect at the upper right corner branch is weak. However, the poster in the lower right corner is purple, due to colour distortion. When we increase the filter radius  $R$ , the halo effect on the tree becomes more and more serious, but the colour distortion of the poster is eliminated. Therefore, in these algorithms, suppression of the halo effect and the colour distortion could not be achieved at the same time. By observing the images in Figures 6(e)–6(g), we can find the results of NLD, AARNCB, and DTMS have similar problems on the halo effect. In Figure 6(l), the proposed algorithm can suppress the halo effect and colour distortion at the same time.

### 4.2 Objective evaluation

In the objective evaluation, the evaluation criteria are dehazing performance and time consumption. The evaluation of dehazing performance can be classified into two categories: no-reference evaluation and full-reference evaluation. The no-reference evaluation is the evaluation of dehazing performance in natural hazy images, and the full-reference evaluation is the evaluation of dehazing performance in synthetic hazy images.

#### 4.2.1 Objective evaluation of dehazing performance

For natural hazy images, there are no real haze-free images for reference. We choose the visual contrast measure (VCM) (Jobson et al., 2006), fog reduction factor (FRF) (Choi et al., 2015; Kansal and Kasana, 2020), and colour naturalness index (CNI) (Huang et al., 2006) as the objective no-reference evaluation metrics for natural images. The VCM and FRF are used to evaluate the performance of dehazing. The CNI is an evaluation metrics for the visual effect of the restored image. In theory, the higher values of VCM, FRF and CNI indicate better dehazing performance and visual effect than others. However, the dehazing process will lead to image distortion in some scenes, such as the sky region. It will introduce new false edges in the distortion region which will affect the correctness of the experimental results. Therefore, we choose four images which without distortion after dehazing for the experiments and exclude the results of FVR. Figure 7 shows the experimental results. The tested images are named forest, pumpkins, train and tree in turn. Table 1,

Table 2 and Table 3 list the quantitative result of the VCM, FRF and CNI, respectively.

**Table 1** Objective evaluation results of VCM on Figure 7

<i>Algorithms</i>	<i>Forest</i>	<i>Pumpkins</i>	<i>Train</i>	<i>Tree</i>
DCP-SM	46.069	43.666	51.423	49.014
DCP-GF	50.702	57.341	56.879	51.987
CAP	46.597	52.746	49.156	52.159
BCCR	53.923	57.137	55.097	61.315
NLD	<i>74.133</i>	<i>74.373</i>	<i>76.620</i>	<i>67.052</i>
AARNCB	66.984	67.483	69.064	61.602
DTMS	48.635	62.207	49.445	48.142
Proposed	57.087	66.570	69.877	61.882

**Table 2** Objective evaluation results of FRF on Figure 7

<i>Algorithms</i>	<i>Forest</i>	<i>Pumpkins</i>	<i>Train</i>	<i>Tree</i>
DCP-SM	0.171	0.255	0.892	0.375
DCP-GF	0.206	0.335	0.885	0.433
CAP	0.125	0.174	0.781	0.337
BCCR	0.205	0.309	0.834	0.494
NLD	0.298	0.398	<i>0.986</i>	<i>0.610</i>
AARNCB	0.235	0.363	0.975	0.505
DTMS	0.265	0.388	0.947	0.516
Proposed	<i>0.305</i>	<i>0.400</i>	0.977	0.605

**Table 3** Objective evaluation results of CNI on Figure 7

<i>Algorithms</i>	<i>Forest</i>	<i>Pumpkins</i>	<i>Train</i>	<i>Tree</i>
DCP-SM	0.804	0.656	<i>0.544</i>	0.705
DCP-GF	0.815	0.622	0.435	0.651
CAP	0.687	0.519	0.372	0.540
BCCR	0.729	0.614	0.359	0.591
NLD	0.992	0.782	0.512	0.866
AARNCB	0.543	0.606	0.479	0.752
DTMS	0.909	0.740	0.493	0.671
Proposed	<i>0.998</i>	<i>0.803</i>	0.500	<i>0.900</i>

As we can see in Table 1 and Table 2, DCP-SM and CAP almost cannot yield high value of metrics VCM and FRF, which indicates that their poor performance in dehazing. The results of NLD produce four higher VCM values. AARNCB and the proposed algorithm rank second and third in the VCM experiment, respectively. The proposed algorithm and NLD both produce two higher FRF values in Table 2. As we can observe in Table 3, the proposed algorithm produces three higher CNI values, which means that the restored images of the proposed algorithm have good visual quality than compared algorithms. In contrast, the proposed algorithm and NLD achieve better dehazing performance than others, and the proposed algorithm has the best visual effects in the compared algorithms.

For synthetic hazy images, the structural similarity index (SSIM) (Wang et al., 2004) and peak signal-to-noise ratio (PSNR) are chosen as full-reference evaluation metrics. High values of SSIM and PSNR indicate that the restored image is similar to the ground truth. In this experiment, we choose several outdoor synthetic images from the RESIDE dataset (Li et al., 2018) as the test input. Figure 8 shows the experimental results for images named bus, temple, flower, and city in turn. Table 4 and Table 5 show the SSIM and PSNR index metrics, respectively. As we can see in Figure 8, the results of DCP-GF, BCCR, NLD and DTMS produce serious image distortion in the sky region which leads to the reduction in the similarity. The proposed algorithm and CAP achieve a better performance than other algorithms.

**Table 4** Objective evaluation results of SSIM on Figure 8

<i>Algorithms</i>	<i>Bus</i>	<i>Temple</i>	<i>Flower</i>	<i>City</i>
DCP-GF	0.888	0.880	0.935	0.879
CAP	<i>0.944</i>	<i>0.949</i>	0.946	<i>0.978</i>
BCCR	0.886	0.829	0.894	0.903
NLD	0.831	0.791	0.924	0.855
AARNCB	0.833	0.827	0.896	0.814
DTMS	0.759	0.809	0.889	0.748
Proposed	0.899	0.929	<i>0.961</i>	0.963

**Table 5** Objective evaluation results of PSNR on Figure 8

<i>Algorithms</i>	<i>Bus</i>	<i>Temple</i>	<i>Flower</i>	<i>City</i>
DCP-GF	14.198	15.148	17.073	15.547
CAP	20.726	17.980	20.353	26.757
BCCR	15.204	15.156	14.700	17.012
NLD	15.938	13.565	15.940	15.752
AARNCB	14.090	15.293	14.076	14.983
DTMS	11.426	12.939	16.902	12.826
Proposed	<i>22.749</i>	<i>19.212</i>	<i>23.398</i>	22.956

#### 4.2.2 Objective evaluation of time consumption

We choose several images with different resolutions for the time consumption experiments, and record the stable data from ten experiments. The average values are reported. Table 5 shows our experimental results. When the image resolution is too high, our experimental conditions would not allow the running of SM, because SM requires a larger memory space to solve a linear system. The proposed algorithm uses FED to solve the P-M equation. The FED scheme can greatly reduce the number of iterations required for a given diffusion time, thus reducing the time consumption. In general, the time consumption of the proposed algorithm is slightly higher than CAP and lower than those of the other compared algorithms.

**Figure 5** Comparison of haze removal results using natural images, (a) hazy image, (b) DCP-SM, (c) DCP-GF, (d) FVR, (e) CAP, (f) BCCR, (g) NLD, (h), AARNCB (i), DTMS, (j) proposed algorithm (see online version for colours)

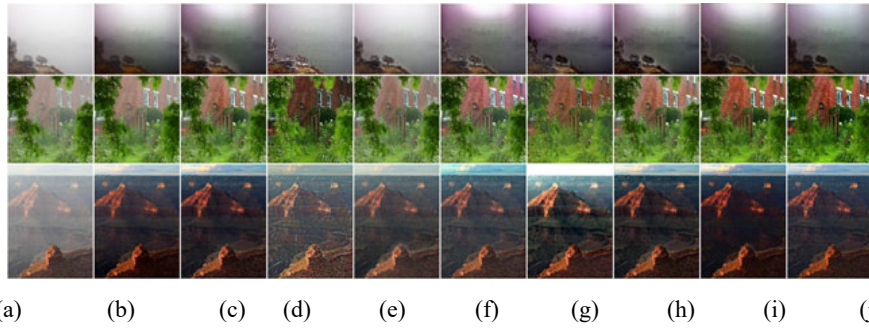


**Figure 6** Comparison of haze removal results with colour distortion, (a) hazy image, (b) DCP-SM, (c) FVR, (d) CAP, (e) NLD, (f) AARNCB, (g) DTMS, (h) DCP-GF, R = 15, (i) DCP-GF, R = 3, (j) BCCR, R = 15, (k) BCCR, R = 3 (l) proposed algorithm (see online version for colours)

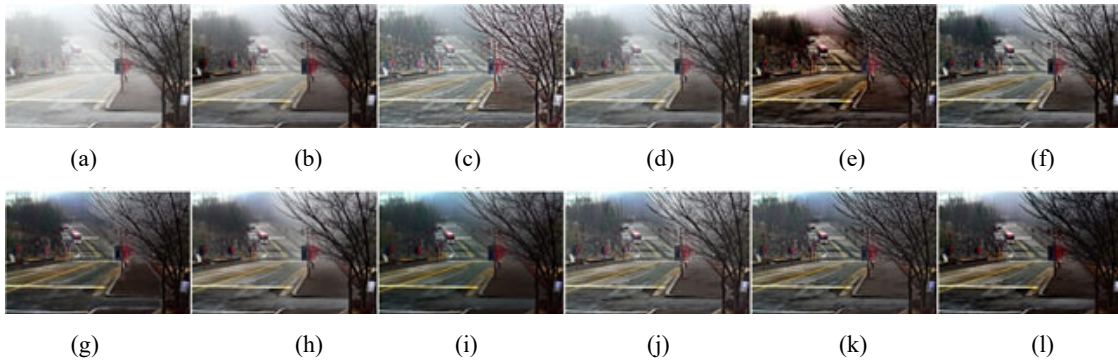


**Figure 7** Comparison of haze removal results using natural images, (a) hazy image, (b) DCP-SM, (c) DCP-GF, (d) CAP, (e) BCCR, (f) NLD, (g) AARNCB, (h) DTMS, (i) proposed algorithm (see online version for colours)

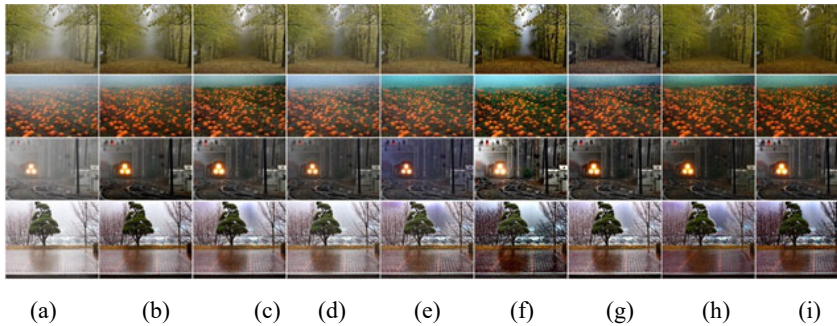


**Figure 8** Comparison of haze removal results using synthetic images, (a) hazy image, (b) ground truth, (c) DCP-GF, (d) CAP, (e) BCCR, (f) NLD, (g) AARNCB, (h) DTMS, (i) proposed algorithm (see online version for colours)

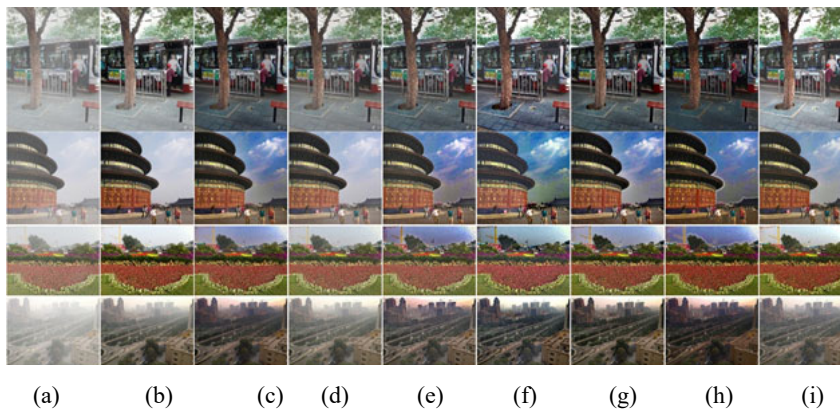


**Table 6** Time consumption (seconds) of different size image

Algorithms	$600 \times 400$	$1,024 \times 768$	$1,556 \times 2,074$
DCP-SM	19.783	65.670	Out of memory
DCP-GF	1.366	4.688	19.057
FVR	1.663	25.408	314.350
CAP	0.542	1.727	7.330
BCCR	1.681	5.572	25.401
NLD	5.184	13.817	38.689
AARNCB	1.016	3.585	17.573
DTMS	2.633	9.207	38.171
Proposed	0.519	2.667	8.307

## 5 Discussion and conclusions

In this paper, we have proposed a novel dual-fusion dehazing algorithm based on anisotropic diffusion and Gaussian filter. The proposed algorithm first used a quadtree search method to estimate atmospheric light. Anisotropic diffusion and Gaussian filter were used to image the minimal component respectively. Considering the characteristics of the atmospheric veil, we proposed a dual-fusion strategy for optimisation. The first image fusion was to correct the colour distortion and the second was to suppress the halo effect on the image depth edge. Then, a simple correction method was used to correct the minimum value of the optimised atmospheric veil, which was to avoid low contrast in the restored image. We also used FED scheme to accelerate the numerical solution of the anisotropic diffusion. The subjective evaluation of the experiment showed that the proposed dehazing algorithm could effectively suppress the halo effect and colour distortion. In the objective evaluation, the proposed algorithm performed better than DCP and other compared algorithms in most of evaluation metrics, and the time consumption was less than that of most the compared algorithms. The proposed dual-fusion strategy can be implemented on a FPGA with a fully pipelined architecture. It can be used in the field of UAV aerial photography and traffic monitoring.

However, even a Gaussian filter with a large standard deviation cannot effectively smooth large size white objects. Therefore, the results of image fusion may be affected. Thus, a robust smooth filter is needed, to improve the performance of the proposed algorithm. In the future work, we will focus on these issues.

## References

Berman, D., Treibitz, T. and Avidan, S. (2020) 'Single image dehazing using haze-lines', *IEEE Transactions on Pattern Analysis and Machine Intelligence*, Vol. 42, No. 3, pp.720–734.

Bui, T.M. and Kim, W. (2018) 'Single image dehazing using color ellipsoid prior', *IEEE Transactions on Image Processing*, Vol. 27, No. 2, pp.999–1009.

Chang, F., Ge, L., Li, S., Wu, K. and Wang, Y. (2021) 'Self-adaptive spatial-temporal network based on heterogeneous data for air quality prediction', *Connection Science*, Vol. 33, No. 3, pp.427–446.

Choi, L.K., You, J. and Bovik, A.C. (2015) 'Referenceless prediction of perceptual fog density and perceptual image defogging', *IEEE Transactions on Image Processing*, Vol. 24, No. 11, pp.3888–3901.

Das, P. and Chand, S. (2021) 'Extracting road maps from high-resolution satellite imagery using refined DSE-LinkNet', *Connection Science*, Vol. 33, No. 2, pp.278–295.

Dhara, S.K., Roy, M., Sen, D. and Biswas, P.K. (2020) 'Color cast dependent image dehazing via adaptive airlight refinement and non-linear color balancing', *IEEE Transactions on Circuits and Systems for Video Technology*, Vol. 31, No. 5, pp.2076–2081.

Ehsan, S.M., Imran, M., Ullah, A. and Elbasi, E. (2021) 'A single image dehazing technique using the dual transmission maps strategy and gradient-domain guided image filtering', *IEEE Access*, Vol. 9, pp.89055–89063.

He, K., Sun, J. and Tang, X. (2010) 'Single image haze removal using dark channel prior', *IEEE Transactions on Pattern Analysis and Machine Intelligence*, Vol. 33, No. 12, pp.2341–2353.

He, K., Sun, J. and Tang, X. (2013) 'Guided image filtering', *IEEE Transactions on Pattern Analysis and Machine Intelligence*, Vol. 35, No. 6, pp.1397–1409.

Huang, K., Wang, Q. and Wu, Z. (2006) 'Natural color image enhancement and evaluation algorithm based on human visual system', *Computer Vision and Image Understanding*, Vol. 103, No. 1, pp.52–63.

Jiang, D., Qu, H., Zhao, J., Zhao, J. and Hsieh, M. (2021) 'Aggregating multi-scale contextual features from multiple stages for semantic image segmentation', *Connection Science*, Vol. 33, No. 3, pp.605–622.

Jobson, D.J., Rahman, Z., Woodell, G.A. and Hines, G.D. (2006) 'A comparison of visual statistics for the image enhancement of FORESITE aerial images with those of major image classes', in *Visual Information Processing XV, International Society for Optics and Photonics*, Vol. 6246, p.624601.

Ju, M., Ding, C., Guo, Y.J. and Zhang, D. (2020) 'IDGCP: image dehazing based on gamma correction prior', *IEEE Transactions on Image Processing*, Vol. 29, pp.3104–3118.

Kansal, I. and Kasana, S.S. (2020) 'Improved color attenuation prior based image de-fogging technique', *Multimedia Tools and Applications*, Vol. 79, Nos. 17–18, pp.12069–12091.

Kholerdi, H.A., TaheriNejad, N., Ghaderi, R. and Baleghi, Y. (2016) 'Driver's drowsiness detection using an enhanced image processing technique inspired by the human visual system', *Connection Science*, Vol. 28, No. 1, pp.27–46.

Kim, J., Jang, W., Sim, J. and Kim, C. (2013) 'Optimized contrast enhancement for real-time image and video dehazing', *Journal of Visual Communication and Image Representation*, Vol. 24, No. 3, pp.410–425.

Land, E.H. and McCann, J.J. (1971) 'Lightness and retinex theory', *Josa*, Vol. 61, No. 1, pp.1–11.

Li, B., Ren, W., Fu, D., Tao, D., Feng, D., Zeng, W. and Wang, Z. (2018) 'Benchmarking single-image dehazing and beyond', *IEEE Transactions on Image Processing*, Vol. 28, No. 1, pp.492–505.

McCartney, E.J. (1976) *Optics of the Atmosphere: Scattering by Molecules and Particles*, John Wiley and Sons, Inc., New York.

- Meng, G., Wang, Y., Duan, J., Xiang, S. and Pan, C. (2013) 'Efficient image dehazing with boundary constraint and contextual regularization', in *Proceedings of the IEEE international Conference on Computer Vision*, pp.617–624.
- Nandal, S. and Kumar, S. (2019) 'Single image fog removal algorithm in spatial domain using fractional order anisotropic diffusion', *Multimedia Tools and Applications*, Vol. 78, No. 8, pp.10717–10732.
- Narasimhan, S.G. and Nayar, S.K. (2002) 'Vision and the atmosphere', *International Journal of Computer Vision*, Vol. 48, No. 3, pp.233–254.
- Perona, P. and Malik, J. (1990) 'Scale-space and edge detection using anisotropic diffusion', *IEEE Transactions on Pattern Analysis and Machine Intelligence*, Vol. 12, No. 7, pp.629–639.
- Seow, M. and Asari, V.K. (2006) 'Ratio rule and homomorphic filter for enhancement of digital color image', *Neurocomputing*, Vol. 69, Nos. 7–9, pp.954–958.
- Sun, X., Wang, Q., Zhang, X., Xu, C. and Zhang, W. (2021) 'Deep blur detection network with boundary-aware multi-scale features', *Connection Science*, pp.1–19 [online] <https://www.tandfonline.com/doi/full/10.1080/09540091.2021.1933906>.
- Tarel, J. and Hautière, N. (2009) 'Fast visibility restoration from a single color or gray level image', in *2009 IEEE 12th International Conference on Computer Vision*, IEEE, pp.2201–2208.
- Tripathi, A.K. and Mukhopadhyay, S. (2012) 'Single image fog removal using anisotropic diffusion', *IET Image Processing*, Vol. 6, No. 7, p.966.
- Wang, Z., Bovik, A.C., Sheikh, H.R. and Simoncelli, E.P. (2004) 'Image quality assessment: from error visibility to structural similarity', *IEEE Transactions on Image Processing*, Vol. 13, No. 4, pp.600–612.
- Wei, H., Dai, Z. and Zuo, Q. (2016) 'A ganglion-cell-based primary image representation method and its contribution to object recognition' *Connection Science*, Vol. 28, No. 4, pp.311–331.
- Wei, Z., Zhu, G., Liang, X., Liu, W. (2020) 'An image fusion dehazing algorithm based on dark channel prior and retinex', *International Journal of Computational Science and Engineering*, Vol. 23, No. 2, pp.115–123.
- Weickert, J., Grewenig, S., Schroers, C. and Bruhn, A. (2016) 'Cyclic schemes for PDE-based image analysis', *International Journal of Computer Vision*, Vol. 118, No. 3, pp.275–299.
- Weickert, J., Romeny, B.M.T.H. and Viergever, M.A. (1998) 'Efficient and reliable schemes for nonlinear diffusion filtering', *IEEE Transactions on Image Processing*, Vol. 7, No. 3, pp.398–410.
- Wu, Z., Gao, Y., Li, L., Xue, J. and Li, Y. (2019) 'Semantic segmentation of high-resolution remote sensing images using fully convolutional network with adaptive threshold', *Connection Science*, Vol. 31, No. 2, pp.169–184.
- Xu, Z. and Zhang, W. (2020) 'Hand segmentation pipeline from depth map: an integrated approach of histogram threshold selection and shallow CNN classification', *Connection Science*, Vol. 32 No. 2, pp.162–173.
- Xu, Z., Liu, X. and Ji, N. (2009) 'Fog removal from color images using contrast limited adaptive histogram equalization', in *2009 2nd International Congress on Image and Signal Processing*, IEEE, pp.1–5.
- Yang, Y., Long, W., Li, Y., Shi, X. and Gao, L. (2021) 'Image defogging based on amended dark channel prior and 4-directional L1 regularisation', *IET Image Processing*, Vol. 15, No. 11, pp.2454–2477.
- Zhao, H., Yao, L., Zeng, Z., Li, D., Xie, J., Zhu, W. and Tang, J. (2021) 'An edge streaming data processing framework for autonomous driving', *Connection Science*, Vol. 33, No. 2, pp.173–200.
- Zhu, Q., Mai, J. and Shao, L. (2015) 'A fast single image haze removal algorithm using color attenuation prior', *IEEE Transactions on Image Processing*, Vol. 24, No. 11, pp.3522–3533.
- Zhu, X., Zuo, J. and Ren, H. (2020) 'A modified deep neural network enables identification of foliage under complex background', *Connection Science*, Vol. 32, No. 1, pp.1–15.